The 1979-2005 Greenland ice sheet melt extent from passive microwave data using an improved version of the melt retrieval XPGR algorithm

X. Fettweis[(1)], J.-P. van Ypersele[(1)], H. Gallée[(2)], F. Lefebre[(3)], W. Lefebvre[(1)]

[(1)] Institut d' Astronomie et de Géophysique Georges Lemaître, Université Catholique de Louvain, 1348 Louvain-la-Neuve, Belgium, fettweis@astr.ucl.ac.be.
[(2)] Laboratoire de Glaciologie et Géophysique de l'Environnement, CNRS, Grenoble, France.
[(3)] Vito - Flemish Institute for Technological Research, Centre for Remote Sensing and Atmospheric Processes, Mol, Belgium.

Abstract

Analysis of passive microwave satellite observations over the Greenland ice sheet reveals a significant increase in surface melt over the period 1979-2005. An improved version of the cross-polarized gradient ratio (XPGR) technique is used to identify the melt and the surface melt acceleration is discussed with results from the regional climate model MAR. From 1979 to 2005, the ablation period increases everywhere over the melt zone except in the regions where the model simulates an heavier summer snowfall. Indeed, more snowfall in summer decreases the liquid water content of the snowpack, raises the albedo and therefore reduces the melt. Finally, the melt acceleration over the Greenland ice sheet is highly correlated with both Greenland and global warming suggesting a continuing surface melt increase in the future.

***Reference** : Fettweis, X., J.-P. van Ypersele, H. Gallée, F. Lefebre, and W. Lefebvre, The 1979–2005 Greenland ice sheet melt extent from passive microwave data using an improved version of the melt retrieval XPGR algorithm, Geophys. Res. Lett., 34, L05502.*

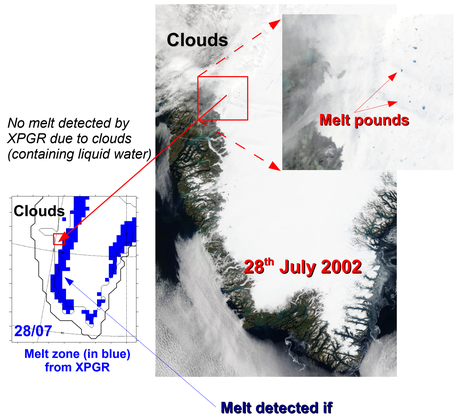

Melt detected if

$$XPGR = \frac{T_b(19H) - T_b(37V)}{T_b(19H) + T_b(37V)} > -0.0158 \Leftrightarrow \text{Liquid water content} > 1\%$$

***Figure 1 :** Satellite photo of the South Greenland taken the 28th of July 2002 from http://modis.gsfc.nasa.gov/gallery/index.php. The melt extent is deduced from the microwave signal (SMMR and SSM/I) by using the **XPGR** technique of Abdalati and Steffen (1997) with the four improvements described hereafter. The XPGR technique compares a normalized difference between the 19-GHz horizontal polarized brightness temperature (**T19H**) and the 37-GHz vertical polarized brightness temperature (**T37V**) with a threshold value to distinguish melt from non-melt points.*

The plot on the left shows that the western ice sheet margin is not detected as melting by XPGR while we can see melt pounds on the photo. The dense clouds visible on the photo are very likely responsible of perturbations in the microwave signal.

Perturbations in the derived microwave melt signal

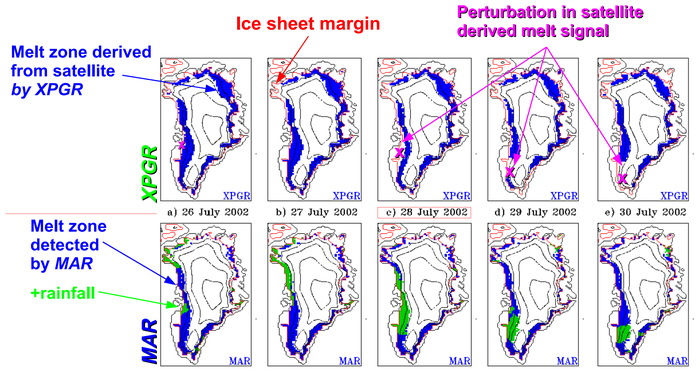

***Figure 2 :** Melt extent (in blue) derived by XPGR and simulated by MAR (bottom row) for different dates in July 2002. The green zones in the MAR fields represent the melt zones where MAR simulates daily liquid precipitation higher than 1 mm/day. A mean liquid water content (LWC) of 1 % by volume in the top meter of snow is used as threshold value to distinguish melt from non-melt points in the MAR simulation.*

• The SSM/I-derived melt patterns do not show melt along the western ice sheet margin while XPGR detects melt higher on the western ablation zone. Moreover, melt is observed on this zone just before and after the 28th July. Finally, MAR detects melt and simulates rainfall in this zone. This leads us to conclude that **rainfall (dense clouds) perturbs the microwave melt signal**. The wavelength of the 37-GHz channel is indeed of the order of the water cloud droplets diameter.

• Therefore, we propose four improvements to the XPGR algorithm to reduce the perturbations in the remote melt signal due to the atmospheric variability (See Fettweis at al. (2006) for more details). The improved XPGR algorithm will be referred hereafter to as **ImpXPGR**.

➢ **Improvement n°1**: We impose the continuity of the melt season to remove gaps shorter than three days between two melting days. The XPGR method aims to detect massive melt and short gaps (due to dense clouds mostly causing liquid precipitation) in the middle of the melt season detected by XPGR are mostly unrealistic.

➢ **Improvement n°2**: Grid points situated at lower altitudes than three adjacent grid points where XPGR detects melt are classified as melting grid points.

➢ **Improvement n°3 and n°4**: A min/max value of T19H is assumed to detected melt/not melt with the aim to remove eventual anomalies in the SMMR-SSM/I brightness temperatures fields. The 19-GHz channel is chosen because it is the least sensitive to the atmospheric variability.

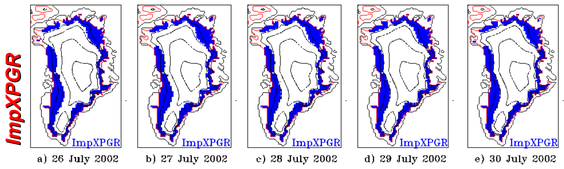

***Figure 3 :** The same as Figure 2 but for ImpXPGR (briefly described above).*

The 1979-2005 Microwave derived surface melt extent

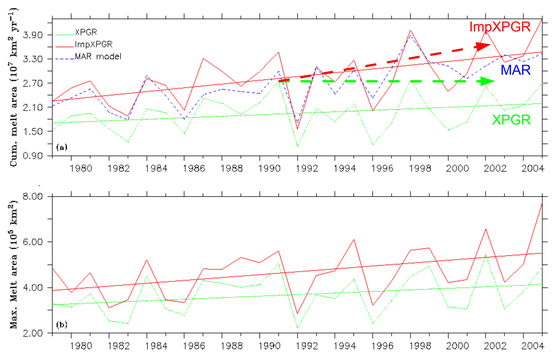

***Figure 4 :** a) Annually cumulated melt area detected by XPGR (dotted), by ImpXPGR (solid) and simulated by MAR (dashed). b) Maximum daily melt extent of the ice sheet. The cumulated melt area is defined as the annual total sum of every daily ice sheet melt area and the maximum melt extent is the maximum extent experiencing at least one melt day.*

• **From 1979, the total increase of the cumulated melt extent** retrieved by XPGR and ImpXPGR in 2005 **is** respectively +0.48x10^7 km^2 (i.e.+28%) and +1.22x10^7 km^2 (i.e.**+54%**) with a significance of 92.0% and 99.5%. The surface melt acceleration is higher by using ImpXPGR because rainfall has also increased during this period which enhances the probability of perturbations in the microwave melt signal.

• Figures 5a-b reveal an **increase of the length of the melt season as well as an expansion of the melt area** on the Greenland ice sheet. The number of melting days increases mainly in the North of Greenland and along the western coast at mid altitude (about near 1500m-2000m).

• At lower altitude **in the western part**, no change occurs because **the melt period extends already all of the melt season** at the beginning of eighties.

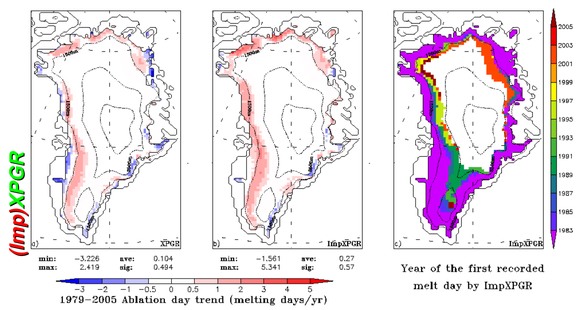

***Figure 5 :** a) Melt trend (in ablation days yr^{-1}) detected by XPGR for the period 1979-2005. b) Idem by ImpXPGR. Minimum (min) and maximum (max) values are indicated below the figures as well as the ice sheet average (ave) and the standard deviation (sig). c) This figure shows an expansion of the largest melt area recorded by ImpXPGR reaching new zones every year.*

• An uniform warming of the ice sheet as shown on Figure 8a would be expected to give an increase of the melt period everywhere on the ice sheet. **The negative trends along the south-eastern coast** in ImpXPGR fields probably **result from heavier snowfall** which decreases the liquid water content of the snow pack, raises the albedo and therefore reduces the melt.

• In the other regions of the Greenland ice sheet, MAR simulates rather a decrease of the snowfall in summer (Figure 8b). Part of this **snowfall decrease results from the warming**, which leads to an increase in the amount of liquid precipitation versus solid precipitation.

•This **increase of rainfall in summer** which **induces enhanced perturbations in the recorded microwave signal** explains why XPGR shows a decrease of the ablation period along the western margin in Figure 5a.

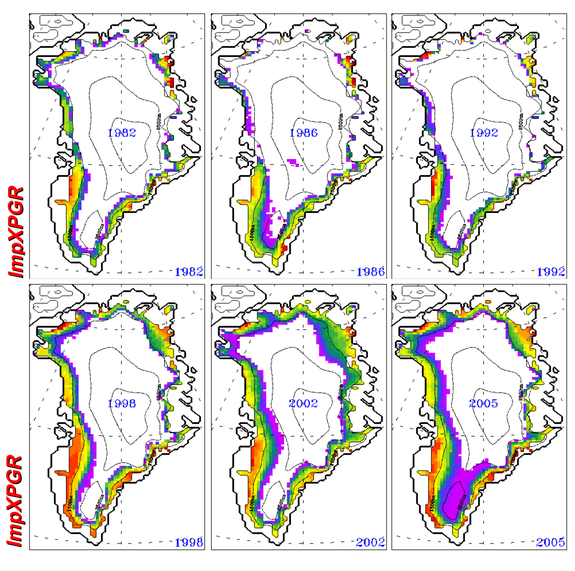

***Figure 6 :** Total number of melt days detected by ImpXPGR for 3 years with a low melt extent and 3 years with a high melt extent. The maximum of melt extent occurs in 2005 followed by 2002 according to Steffen et al. (2004). The South-Dome at an elevation of 2900 m is reached in 2005. The minimum occurs in 1992 due to the eruption of the Mount Pinatubo. See http://www.climate.be/u/fettweis for an animation of these plots.*

Model description

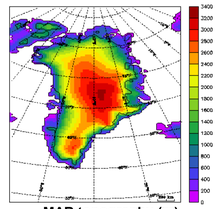

Begin	01/09/1978	
End	31/12/2005	
Simulated domain	2000 km x 3750 km	
Resolution	25 km	
1st level	3 m	
Time step	120 s	
Boundaries forcing	ECMWF-ERA 6-hourly	
Vertical levels	Atmosphere	30
	Snow	20
	Tundra	7
Ocean	ERA SST	
Sea-ice	ERA Sea-ice	

We use results from the regional climate atmospheric **MAR model** (Gallée and Schayes, 1994) coupled to a snow model. The simulation starts in September 1978 and lasts until December 2005 with a spatial resolution of 25 km. The ERA-40 reanalysis (1977-2002) and after that, the operational analysis (2002-2005) from the European Centre for Medium-Range Weather Forecasts are used to initialize the meteorological fields at the beginning of the simulation and to force the lateral boundaries every 6 hours. The schemes and the set-up used here are fully described in Fettweis et al. (2005, 2006).

Model Results

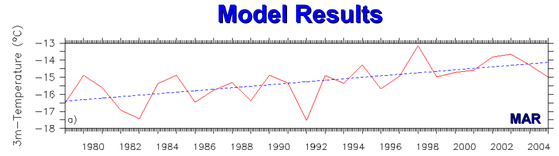

***Figure 7 :** Time series of the summer (from 1st May to 30th September) total ice sheet temperature average simulated by MAR (in °C summer^{-1}).*

• **Since 1979, the MAR model simulates an increase of the mean ice sheet summer temperature of +2.4°C**. This modelled warming shown on Figure 8 is larger at the top of the ice sheet than along the ice sheet margin because the surface temperature of melting snow/ice is limited to 0°C. The correlation between the average ice sheet summer MAR temperature and the cumulated melt extent retrieved by XPGR and ImpXPGR is respectively 0.66 and 0.77.

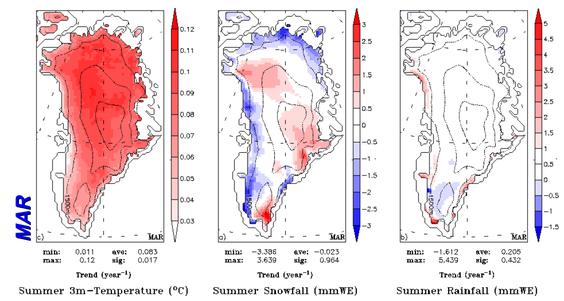

***Figure 8 :** a) 27-year linear regression change of the 3m-temperature simulated by MAR in summer (1st May to 30th September). b) Idem for snowfall. c) Idem for rainfall.*

Conclusion

These results, in agreement with the recent Gravity Recovery and Climate Experiment (GRACE) measurements, suggest that the **melt at the surface of the Greenland ice sheet is significantly increasing and will** very likely **continue to increase in the future** following the global warming. The **correlation with the global mean temperature** from the Climatic Research Unit (CRU) and the annually cumulated melt area derived by ImpXPGR **is 0.71** over the period 1979-2005. **This will have an obvious impact of the Greenland ice sheet mass balance** if the precipitation is not increasing in the same proportion and if the melt water-induced ice flow acceleration observed by Zwally et al. (2002) is confirmed in the future.

References

Abdalati, W. and K. Steffen: Snowmelt on the Greenland ice sheet as derived from passive microwave satellite data, *J. Climate*, 10: 165-175, 1997.

Fettweis, X., Gallée, H., Lefebre, L., van Ypersele, J.-P. (2005), Greenland surface mass balance simulated by a regional climate model and comparison with satellite derived data in 1990-1991, *Clim. Dyn.*, 24, 623-640.

Fettweis, X., Gallée, H., Lefebre, L., van Ypersele, J.-P. (2006), The 1988-2003 Greenland ice sheet melt extent by passive microwave satellite data and a regional climate model, *Clim. Dyn.*, 27, 5, 531-541.

Fettweis, X., J.-P. van Ypersele, H. Gallée, F. Lefebre, and W. Lefebvre (2007), The 1979–2005 Greenland ice sheet melt extent from passive microwave data using an improved version of the melt retrieval XPGR algorithm, *Geophys. Res. Lett.*, 34, L05502.

Gallée, H. and G. Schayes (1994), Development of a three-dimensional meso-γ primitive equations model, *Mon. Wea. rev.*, 122, 671-685.

Steffen, K., S. V. Nghiem, R. Huff, and G. Neumann (2004), The melt anomaly of 2002 on the Greenland Ice Sheet from active and passive microwave satellite observations, Geophys. Res. Lett., 31, L20402.

Zwally, J.H., W. Abdalati, T. Herring, K. Larson, J. Saba, and K. Steffen (2002), Surface Melt-Induced Acceleration of Greenland ice sheet Flow, *Science*, 297, 218-222.

Acknowledgements

The authors acknowledge the National Snow and Ice Data Center (NSIDC, Boulder, Colorado) for providing the passive microwave satellite data from Scanning Multichannel Microwave Radiometer (SMMR) [1979-1987] and Special Sensor Microwave/Imager (SSM/I) [1987-2005] (see http://nsidc.org).